Synthesis, Structure, and Single-Crystal EPR Study of $[Cp(t\text{-}Bu_3PN)Ti(\mu\text{-}Cl)]_2$

Raymond C. W. Sung, Silke Courtenay, Bruce R. McGarvey,* and Douglas W. Stephan*

Chemistry and Biochemistry, School of Physical Sciences, University of Windsor, Windsor, Ontario, Canada N9P 3P4

Received November 8, 1999

The reduction of $CpTi(NPt\text{-}Bu_3)Cl_2$ with Mg powder in benzene proceeds slowly to give $[CpTi(NPt\text{-}Bu_3(\mu\text{-}Cl)]_2$ (**1**). An X-ray crystallographic study confirmed **1** is a centrosymmetric chloro-bridged dimer in the solid state. A single-crystal EPR study of **1** permitted the determination of the best-fitted values for the diagonal spin Hamiltonian parameters. This appears to be the first EPR single-crystal study of a Ti(III)−Ti(III) dimer. The implications of these data are considered and discussed in light of extended Hückel molecular orbital calculations.

Introduction

Much of the currently ongoing development of transition-metal chemistry is stimulated by the potential for new commercial polymerization catalysts. Recently, efforts to employ alternatives to the now conventional cyclopentadienyl ligands have been pioneered by the research groups of Brookhart,[1−7] Gibson,[8,9] McConville,[10,11] Schrock,[12−14] and others.[15−18] In our own work, we have recently reported the discovery of the highly effective catalysts of the forms $CpTi(NPR_3)X_2$ and $(R_3PN)_2TiX_2$. Our initial strategy for selection of phosphinimide ligands was based on the similarity of the steric analogy of these ligands to cyclopentadienyl ligands.[19,20] In this paper, we approach the question of the electronic characteristics of Ti−phosphinimide complexes via an examination of related Ti(III) derivatives. Herein, we describe the synthesis and structure of the Ti(III) dimer $[CpTi(NPt\text{-}Bu_3)(\mu\text{-}Cl)]_2$ (**1**). In addition, we report the first single-crystal EPR study of a Ti(III)−Ti(III) dimer. The implications of these data are considered and discussed in light of extended Hückel molecular orbital calculations.

Experimental Section

General Data. All preparations were done under an atmosphere of dry, O_2-free N_2 employing both Schlenk line techniques and an Innovative Technologies or Vacuum Atmospheres inert atmosphere glovebox. Solvents were purified employing Grubb-type columns manufactured by Innovative Technology. EPR spectra were recorded using an X-band Bruker ESP 300E spectrometer. Guelph Chemical Laboratories Inc., Guelph, Ontario, performed combustion analyses. $CpTi(NPt\text{-}Bu_3)Cl_2$ was prepared as previously described.[19]

Synthesis of $[CpTi(NPt\text{-}Bu_3)(\mu\text{-}Cl)]_2$ (1). To a solution of $CpTi(NPt\text{-}Bu_3)Cl_2$ (400 mg, 0.99 mmol) in benzene was added Mg powder (50 mg, 2.05 mmol). The reaction mixture was stirred for 2 weeks and filtered, and the solvent was evaporated, isolating the red-brown product in 69% yield. Anal. Calcd for $C_{17}H_{32}PNTiCl$: C, 51.02; H, 8.06; N, 3.50. Found: C, 50.98; H, 7.97; N, 3.38.

X-ray Data Collection and Reduction. X-ray-quality crystals of **1** were obtained directly from the preparation as described above. The crystal was manipulated and mounted in a capillary in a glovebox, thus maintaining a dry, O_2-free environment. Diffraction experiments were performed on a Siemens SMART System CCD diffractometer collecting a hemisphere of data in 1329 frames with 10 s exposure times. Crystal data are summarized in Table 1. The observed extinctions were consistent with the space group. The data set was collected ($4.5° < 2\theta < 45−50.0°$). A measure of decay was obtained by recollecting the first 50 frames of each data set. The intensities of reflections within these frames showed no statistically significant change over the duration of the data collections. The data were processed using the SAINT and XPREP processing package. An empirical absorption correction based on redundant data was applied to the data set. Subsequent solution and refinement was performed using the SHELXTL solution package operating on a SGI Indy computer.

Structure Solution and Refinement. Non-hydrogen atomic scattering factors were taken from the literature tabulations.[21] The heavy

(1) Mitchell, J. P.; Hajela, S.; Brookhart, S. K.; Hardcastle, K. I.; Henling, L. M.; Bercaw, J. E. *J. Am. Chem. Soc.* **1996**, *118*, 1045−1053.
(2) Rix, F. C.; Brookhart, M.; White, P. S. *J. Am. Chem. Soc.* **1996**, *118*, 4746−4764.
(3) Killian, C. M.; Johnson, L. K.; Brookhart, M. *Organometallics* **1997**, *16*, 2005−2007.
(4) Mecking, S.; Johson, L. K.; Wang, L.; Brookhart, M. *J. Am. Chem. Soc.* **1998**, *120*, 888−899.
(5) Killian, C. M.; Tempel, D. J.; Johnson, L. K.; Brookhart, M. *J. Am. Chem. Soc.* **1996**, *118*, 11664−11665.
(6) Johnson, L. K.; Mecking, S.; Brookhart, M. *J. Am. Chem. Soc.* **1996**, *118*, 267−268.
(7) Johnson, L. K.; Killian, C. M.; Brookhart, M. *J. Am. Chem. Soc.* **1995**, *117*, 6414−6415.
(8) Coles, M. P.; Dalby, C. I.; Gibson, V. C.; Clegg, W.; Elsegood, M. R. J. *Chem. Commun.* **1995**, 1709.
(9) Gibson, V. C.; Marshall, E. L.; Redshaw, C.; Clegg, W.; Elsegood, M. R. J. *J. Chem. Soc. D* **1996**, *021*, 4197.
(10) Scollard, J. D.; McConville, D. H. *J. Am. Chem. Soc.* **1996**, *118*, 10008−10009.
(11) Scollard, J. D.; McConville, D. H.; Vittal, J. J. *Organometallics* **1995**, *14*, 8.
(12) Baumann, R.; Davis, W., M.; Schrock, R. R. *J. Am. Chem. Soc.* **1997**, *119*, 3830−3831.
(13) Schrock, R. R.; Luo, S.; Lee, J. C.; Zanetti, N. C.; Davis, W. M. *J. Am. Chem. Soc.* **1996**, *118*, 3883−3895.
(14) Warren, T. H.; Schrock, R. R.; Davis, W. M. *Organometallics* **1998**, *17*, 308−321.
(15) Littke, A.; Sleiman, N.; Bensimon, C.; Richeson, D. S.; Yap, G. P. A.; Brown, S. J. *Organometallics* **1998**, *17*, 446−451.
(16) Bazan, G. C.; Donnelly, S. J.; Ridriguez, G. *J. Am. Chem. Soc.* **1995**, *117*, 2671−2672.
(17) Bazan, G. C.; Rodriguez, G.; Ashe, A. J., III.; Al-Ahmad, S.; Muller, C. *J. Am. Chem. Soc.* **1996**, *118*, 2291−2292.
(18) Kretschmer, W. P.; Troyanov, S. I.; Meetsma, A.; Hessen, B.; Teuben, J. H. *Organometallics* **1998**, *17*, 284−286.
(19) Stephan, D. W.; Stewart, J. C.; Guerin, F.; Spence, R. E. v.; Xu, W.; Harrison, D. G. *Organometallics* **1999**, *17*, 1116−1118.
(20) Stephan, D. W.; Guerin, F.; Spence, R. E. v.; Koch, L.; Gao, X.; Brown, S. J.; Swabey, J. W.; Wang, Q.; Xu, W.; Zoricak, P.; Harrison, D. G. *Organometallics* **1999**, *17*, 2046−2048.
(21) Cromer, D. T.; Mann, J. B. *Acta Crystallogr., Sect. A* **1968**, *A24*, 390.

10.1021/ic991305l CCC: $19.00
Published on Web 05/20/2000

Table 1. Crystallographic Data for **1**[a]

empirical formula	$C_{23}H_{40}ClNPTi$	fw	444.88
temp (K)	293(2)	wavelength (Å)	0.71073
cryst syst	triclinic	space group	*P*-1
a (Å)	9.182(2)	*b* (Å)	11.283(3)
c (Å)	11.437(3)	α (deg)	76.72(2)
β (deg)	78.84(2)	*γ* (deg)	81.02(2)
vol (Å^3), *Z*	1123.7(5), 2	*ρ*(calcd) (Mg/m^3)	1.315
μ (mm^{-1})	0.580	R1 [$I > 2\sigma(I)$]	0.0438
wR2	0.1220		

[a] $R = \sum||F_o| - |F_c||/\sum|F_o|$, $wR2 = [\sum(|F_o| - |F_c|)^2|/\sum|F_o|^2]^{0.5}$.

atom positions were determined using direct methods employing the SHELXTL direct method routines. The remaining non-hydrogen atoms were located from successive difference Fourier map calculations. The refinements were carried out by using full-matrix least-squares techniques on *F*, minimizing the function $w(|F_o| - |F_c|)^2$, where the weight *w* is defined as $4F_o^2/2\sigma(F_o^2)$ and F_o and F_c are the observed and calculated structure factor amplitudes. In the final cycles of refinement, all non-hydrogen atoms were assigned anisotropic temperature factors. Carbon-bound hydrogen atom positions were calculated and allowed to ride on the carbon to which they are bonded assuming a C−H bond length of 0.95 Å. Hydrogen atom temperature factors were fixed at 1.10 times the isotropic temperature factor of the carbon atom to which they are bonded. The hydrogen atom contributions were calculated, but not refined. The final values of refinement parameters are given in Table 1. The locations of the largest peaks in the final difference Fourier map calculation as well as the magnitude of the residual electron densities in each case were of no chemical significance. Positional parameters, hydrogen atom parameters, thermal parameters, and bond distances and angles have been deposited as Supporting Information.

EHMO Calculations. These calculations were performed employing the molecular modeling and computational software package CACHE. The computational model $CpTi(NPH_3)Cl_2$ was constructed employing the MM3 parameter set. The geometry was then adjusted in accord with the basic geometric parameters found on the basis of the crystallographic data reported herein for **1**. Phosphinimide substituents were replaced by hydrogen for computational and interpretation simplicity.

Single-Crystal EPR Study. Over a 6 month period in a drybox, a large single crystal of **1** was obtained. The crystal was enveloped in epoxy for manipulation outside of the drybox. Single-crystal measurements at room temperature were done using an X-band Bruker ESP 300E spectrometer equipped with an electromagnet capable of providing a magnetic field from 50 G to 15 kG, a gaussmeter, a microwave counter, and an accurate single-axis crystal rotator. A crystal of size about 3 × 5 × 2 mm was embedded in epoxy resin and fixed inside a detachable custom-made plexiglass cube. EPR spectra were recorded every 6° over a 180° rotation in each of the three orthogonal planes defined by the plexiglass cube. The 0° of each rotation was defined as the orientation of the magnetic field when perpendicular to one face of the cube. This orientation was first estimated visually and then corrected by making use of the fact that each rotation intersects the other two rotations 90° apart. These corrections to the visual estimate were no more than 7°. Typical measurement conditions were microwave power 20 mW, microwave frequency 9.7 GHz, modulation amplitude 3.830 G, and 4 K data points covering a sweep width of 4000 G. However, VT EPR experiments on a single crystal of **1** were not performed because the crystal of **1** decomposed after the several weeks necessary for the single-crystal EPR experiments. Numerous repeated efforts to obtain suitable, large single crystals were unsuccessful.

Results and Discussion

Synthesis and Structure. The reduction of $CpTi(NPt\text{-}Bu_3)Cl_2$[19] was attempted under a variety of conditions. In general, reactions with reductants such as $LiAlH_4$, super-hydride, borohydride, Mg, Zn, and BuLi in THF appear to proceed quickly, yet give mixtures of products. In contrast, reaction of $CpTi(NPt\text{-}Bu_3)Cl_2$ with Mg powder in benzene proceeds slowly but cleanly over a 2−3 week period at 25 °C. In this manner, the red-brown species $[CpTi(NPt\text{-}Bu_3)(\mu\text{-}Cl)]_2$ (**1**) was prepared and isolated in 69% yield. Although a dimeric formulation for **1** was anticipated, solution EPR spectra were indicative of a singlet spin system, suggesting dissociation affords a monomeric species in solution. Thus, our attention focused on the nature of **1** in the solid state. An X-ray crystallographic study confirmed **1** is a centrosymmetric chloro-bridged dimer (Figure 1) in the solid state. The coordination spheres of the Ti centers are comprised of a cyclopentadienyl ring, a phosphinimide ligand, and two chloride atoms that bridge to the second Ti center. The Ti_2Cl_2 core is planar with equivalent Ti−Cl distances of 2.4840(11) and 2.4839(10) Å. These distances are significantly shorter than those seen in $[Cp_2Ti(\mu\text{-}Cl)]_2$ (2.559(4)−2.585(4) Å), $[(C_5H_4Me)_2Ti(\mu\text{-}Cl)]_2$ (2.526(2)−2.566(2) Å),[22] $(Cp_2Ti(\mu\text{-}Cl))_2Mg(THF)_2$ (2.568(2), 2.565(2) Å), and $(Cp_2Ti(\mu\text{-}Cl)_2Mg(THF)_2(\mu\text{-}Cl))_2$ (2.535(5), 2.556(6) Å).[23] The Ti−Cl−Ti′ and Cl−Ti−Cl′ angles about the core are 95.11(4)° and 84.89(4)°, respectively. These angles compare to those seen in the Ti(III) dimer $[Cp_2Ti((\mu\text{-}PMe_2)]_2$ (96.5(1)°, 83.3(1)°).[24] The Ti−N and P−N distances are 1.820(2) and 1.576(2) Å in **1**, respectively. While the P−N distance in **1** is comparable with those seen in $(t\text{-}Bu_3PN)_2TiCl_2$ (P−N, 1.579(4), 1.561(3) Å; Ti−N, 1.789(4), 1.792(4) Å),[20] the Ti−N distance in **1** is significantly longer, consistent with the Ti(III) oxidation state.

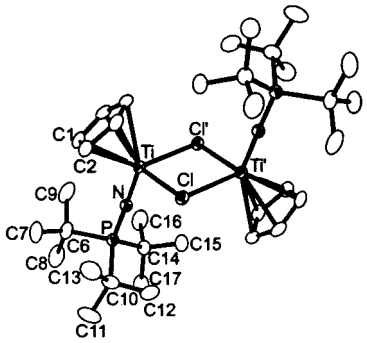

Figure 1. ORTEP drawings of **1**. The 30% thermal ellipsoids are shown. Hydrogen atoms have been omitted for clarity. Ti−N(1) 1.820(2); Ti−Cl 2.4839(10); Ti−Cl′ 2.4840(11); P−N 1.576(2); N−Ti−Cl′ 104.97(8); N−Ti−Cl 105.30(8); Cl′−Ti−Cl 84.89(4); Ti′−Cl−Ti 95.11(4); P−N−Ti 172.1(2).

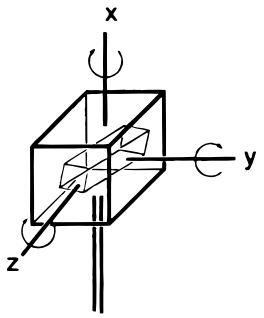

Figure 2. Schematic of the plexiglass crystal mount.

Single-Crystal EPR Study. X-band single-crystal EPR measurements were done at room temperature with a large crystal embedded in epoxy resin and fixed inside a detachable custom-made plexiglass cube (Figure 2). The spectrum (Figure 3) shows the typical features of an $S = 1$ system in one of the

(22) Jungst, R.; Sekutowski, D.; Davis, J.; Luly, M.; Stucky, G. *Inorg. Chem.* **1977**, *16*, 1645−1655.
(23) Stephan, D. W. *Organometallics* **1992**, *11*, 996.
(24) Dick, D. G.; Stephan, D. W. *Can. J. Chem.* **1991**, *69*, 1146−1152.

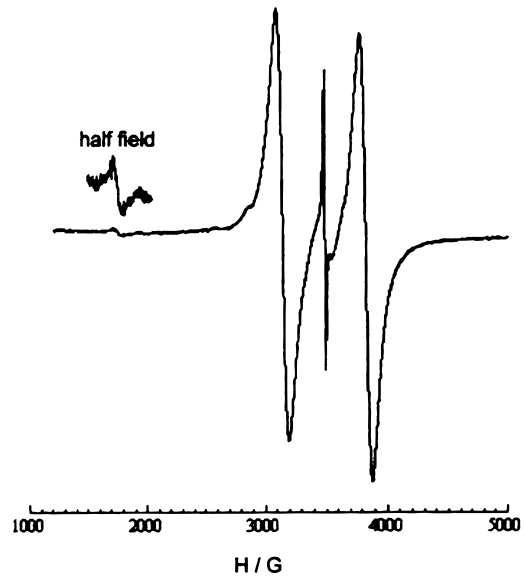

Figure 3. X-band single-crystal EPR of **1**.

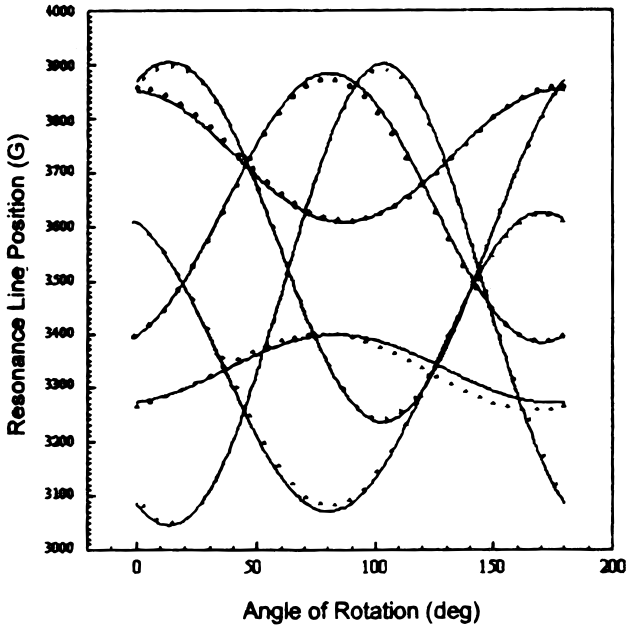

Figure 4. Angular dependence of the two main resonance lines for all three rotation planes and the best-fitted values for the diagonal spin Hamiltonian parameters.

rotation planes. The resonance lines at about 3142 and 3826 G are attributable to the $|0\rangle \rightarrow |1\rangle$ and $|-1\rangle \rightarrow |0\rangle$ transitions, respectively, and the half-field line at about 1743 G results from the $|-1\rangle \rightarrow |1\rangle$ transition. The center line at about 3486 G is due to the presence of a small amount of Ti^{3+} impurities. The angular dependence of the $|0\rangle \rightarrow |1\rangle$ and $|-1\rangle \rightarrow |0\rangle$ resonance lines in the three orthogonal rotation planes were fitted using the exact solutions of the spin Hamiltonian

$$\hat{H} = \beta_e \hat{\mathbf{S}} \cdot \mathbf{g} \cdot \mathbf{H} + D[\hat{S}_z^2 - {}^1/_3 S(S+1)] + E(\hat{S}_x^2 - \hat{S}_y^2) \qquad (1)$$

A computer program was written to simulate the angular dependence of the two main resonance lines for all three rotation planes which are designated as the *xy*, *xz*, and *yz* planes in our laboratory coordinate system. The results (Figure 4) and the best-fitted values for the spin Hamiltonian parameters are given in Table 2. Although the absolute sign of *D* was not determined, it is known that *D* and *E* are of the same sign. The choice of sign given in Table 2 is explained below. Equation 1 assumes the principal axes of the **g** and **D** matrices are colinear, and the excellence of our fitting suggests that this is basically correct for this system.

Table 2. EPR Parameters of $Ti^{3+}-Ti^{3+}$ Dimers

compd	g_x	g_y	g_z	D (cm^{-1})	E (cm^{-1})
1	1.971(1)	1.938(1)	1.993(1)	−0.0413(1)	−0.0063(1)
3[a]	1.980	1.964	2.001	−0.0446	0.0069
4[a]	1.976	1.958	1.997	−0.0463	0.0066
5[a]	1.98	1.97	2.00	−0.037	∼0.000
6[b]	1.984	1.969	1.992	−0.0124	0.0018
7[b]	1.977	1.974	1.981	−0.0271	0.0017

[a] Reference 31. **3** = $[(Cp)_2Ti(\mu\text{-}OCH_3)]_2$; **4** = $[(Cp)_2Ti(\mu\text{-}OC_2H_5)]_2$; **5** = $[(Cp)_2TiCl]_2$. [b] Reference 26. **6** = $[(Cp)_2Ti]_2$(2,2′-biimidazole); **7** = $[(Cp)_2Ti(pyrazole)]_2$.

To our knowledge, the present work is the first EPR single-crystal study of a Ti(III)−Ti(III) dimer. There have been earlier frozen solution studies of many Ti(III)−Ti(III) dimers that have much larger Ti−Ti distances.[25−30] The most recent study by Samuel et al.[31] deals with dimers having methoxo, ethoxo, and chloro bridges and zero-field interactions similar to that seen for **1**. Spin Hamiltonian parameters are listed in Table 2 from these earlier studies for systems in which the Ti−Ti distance is known, for comparison. The *x* and *y* labels have been interchanged to conform with our choice of axes. The values for the chloro-bridged complex are approximate due to the poor resolution in the spectrum. The larger magnitudes for *D* in the alkoxide-bridged complexes are primarily due to the shorter Ti−Ti distances in these dimers. The *g* values are similar except for the markedly lower value for g_y in **1**.

Analysis of the zero-field parameters, *D* and *E*, for related Cu(II)−Cu(II)[32,33] and VO(IV)−VO(IV)[28] dimers has considered two contributions to *D* and *E*:

$$D = D_d + D_e; \qquad E = E_d + E_e \qquad (2)$$

D_d and E_d are contributions from the point dipolar interaction of two spins at the two metal sites. D_e and E_e are the contributions from the anisotropy in the exchange interaction resulting from spin−orbit mixing of excited states into the ground state. It is customary to calculate the dipolar terms from X-ray data and estimate the exchange contribution from eq 2. The equations used to calculate these dipolar terms are simple but have been incorrectly given in some of the literature, for example, in Samuel *et al.*[31] For this reason, we will indicate how our equations were derived. The basic dipole−dipole interaction term is

$$H_{ss} = (\beta^2/R^3)[-2g_z^2 s_{1z} s_{2z} + g_x^2 s_{1x} s_{2x} + g_y^2 s_{1y} s_{2y}] \qquad (3)$$

(25) Corbin, D. R.; Francesconi, L. C.; Hendrickson, D. N.; Stucky, G. D. *Inorg. Chem.* **1981**, *20*, 2084−2089.
(26) Feiselmann, B. F.; Hendrickson, D. N.; Stucky, G. D. *Inorg. Chem.* **1978**, *17*, 2078−2084.
(27) Feiselmann, B. F.; Hendrickson, D. N.; Stucky, G. D. *Inorg. Chem.* **1978**, *17*, 1841−1848.
(28) Sekutowski, D.; Jungst, R.; Stucky, G. D. *Inorg. Chem.* **1978**, *17*, 1848−1855.
(29) Francesconi, L. C.; Corbin, D. R.; Clauss, A. W.; Hendrickson, D. N. *Inorg. Chem.* **1981**, *20*, 2078−2083.
(30) Francesconi, L. C.; Corbin, D. R.; Clauss, A. W.; Hendrickson, D. N.; Stucky, G. D. *Inorg. Chem.* **1981**, *20*, 2059−2069.
(31) Samuel, E.; Harrod, J. F.; Gourier, D.; Dromzee, Y.; Robert, F.; Jeannin, Y. *Inorg. Chem.* **1992**, *31*, 3252.
(32) Ozarowski, A.; Reinen, D. *Inorg. Chem.* **1986**, *25*, 1704−1708.
(33) Boillot, M.; Journaux, Y.; Bencini, A.; Gatteschi, D.; Kahn, O. *Inorg. Chem.* **1985**, *24*, 263.

Table 3. Factoring of Zero-Field Parameters for $Ti^{3+}-Ti^{3+}$ Dimers into Dipole and Exchange Contributions (cm^{-1})

	1	**3**	**4**	**6**	**7**
D	−0.0413	−0.0446	−0.0463	−0.0124	−0.0271
E	−0.0063	−0.0069	−0.0066	0.0018	0.0017
D_d	−0.0343	−0.0455	−0.0453	−0.0078	−0.0208
E_d	0.0003	0.0002	0.0002	0.0000	0.0000
D_e	0.0134	−0.0111	0.0107	0.0050	−0.0063
E_e	−0.0002	0.0031	0.0029	0.0014	0.0017
exchange axis[a]	*y*	*x*	*y*	*x*	*z*
R (Å)	3.666	3.35	3.35	6.02	4.339

[a] Principal exchange axis.

where R is the metal−metal distance along the z axis and β is the Bohr magneton. For the $S = 1$ system D_d is the difference between the $\langle 11|H_{ss}|11\rangle$ and $\langle 10|H_{ss}|10\rangle$ matrix elements, while $E_d = \langle 11|H_{ss}|1\ -1\rangle$. The resulting equations are

$$D_d = (\beta^2/2R^3)[g_z^2 + {}^1/_2(g_x^2 + g_y^2)] \quad (4)$$

$$E_d = (\beta^2/4R^3)[g_z^2 - g_y^2] \quad (5)$$

The values of D, E, D_d, E_d, D_e, and E_e are given in Table 3 for **1** and the others listed in Table 2. It is expected that the D_d term will dominate in the Ti(III)−Ti(III) dimers, and this is confirmed by the closeness in the magnitude between the experimental and dipolar values of D. This means the negative values can be assigned to D in Table 2, and we can identify the z axis in our coordinate system as the Ti−Ti axis.

The D_e and E_e values in Table 3 are not the simple differences obtained from eq 2, but have been converted to a different coordinate system to determine the major distortion axis for the zero-field interaction. The parameters D and E are defined in terms of differences between the zero-field interactions for the three principal axes of the system. It is customary to choose as the z axis the main distortion direction, so that D is greater than E. When this is the case, $|E| \leq |D/3|$. For compound **1** eq 2 yields values of $D_e = -0.0070$ and $E_e = -0.0066$, so we know that the major distortion for the exchange interaction is not along the z axis we have chosen. If we choose our x axis to be the distortion direction, we get $D_e = -{}^1/_2(-0.0070) - {}^3/_2(-0.0066) = 0.0134$ and $E_e = -{}^1/_2(-0.0070) - {}^1/_2(-0.0066) = -0.0002$, which means that the major difference in the exchange interaction is along our x axis. The corresponding calculation for the y axis gives $D_e = -{}^1/_2(-0.0070) + {}^3/_2(-0.0066) = 0.0064$ and $E_e = -{}^1/_2(-0.0070) - {}^1/_2(-0.0066) = 0.0068$. The same calculations were carried out for the other compounds in Table 3 to give the exchange values listed. The axis assigned to D_e is also listed in the table. In the alkoxide-bridged complexes,[31] $|E_e| \approx |D_e/3|$ and therefore no unique direction exists for this interaction. The major distortion direction for the exchange interaction being perpendicular to the Ti−Ti direction is not unique, as is found for Cu(II)−Cu(II)[32,33] dimers and for VO(IV)−VO(IV)[32] dimers. What is different in **1** is that the major distortion direction for the **g** tensor (y axis) is different from that for the exchange anisotropy (x axis). The two axes are the same for the copper and vanadyl dimers. This matter is discussed further after the **g** tensor is considered.

Samuel *et al.*[31] have pointed out that the near-C_{2v} symmetry of the Ti(III)−Ti(III) dimers results in a ground state that is a mixture of d_{z^2} and $d_{x^2-y^2}$ which can be written as

$$a(d_{z^2}) + b(d_{x^2-y^2}) \quad (6)$$

because both orbitals belong to the same irreducible representation A_1. Second-order perturbation theory then gives for the principal g values the equations

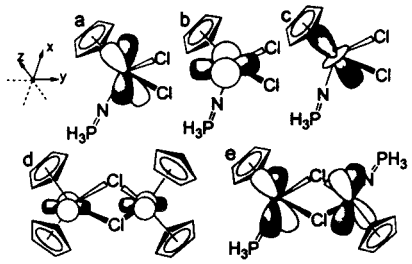

Figure 5. (a−c) LUMOs of the $CpTi(NPH_3)Cl_2$. (d) HOMO for the dimer $[Cp_2Ti(\mu\text{-}Cl)]_2$. (e) HOMO for the dimer $[CpTi(NPH_3)(\mu\text{-}Cl)]_2$.

$$\Delta g_x = 2\lambda(\sqrt{3}a + b)^2/\Delta E_{yz}$$

$$\Delta g_y = 2\lambda(\sqrt{3}a - b)^2/\Delta E_{xz} \quad (7)$$

$$\Delta g_z = 8\lambda b^2/\Delta E_{xy}$$

in which $\Delta g_x = 2.0023 - g_x$, etc. Assuming $\Delta E_{xz} = \Delta E_{yz}$, the following values are calculated from Δg_x and Δg_y: $a = 0.96$, $b = -0.28$, $\lambda/\Delta E = 0.0088$. These values give $g_z = 1.996$, which is not too different from the experimental value. Although these numbers make it appear that the ground state is mainly d_{z^2}, it must be pointed out that if $b = -0.5$ the ground state would best be described as $d_{z^2-x^2}$, which is a $d_{x^2-y^2}$-type orbital perpendicular to the y axis. Thus, the ground state has most of the electron density located in the xz plane along the x and z axes. However, it is not known which axis, x or y, is in the $TiCl_2Ti$ plane. Below arguments are presented that support the fact that y is the axis in the $TiCl_2Ti$ plane.

Most workers in this field have used a spin−orbit theory that connects the exchange interaction with elements of the theory for the **g** tensor, which takes the form

$$D_{ij} = \sum_n [\lambda^2 \langle 0|l_i|n\rangle\langle n|l_j|0\rangle/E_n^2] \quad (8)$$

where D_{ij} are the nine elements of the zero-field matrix and i and j refer to the three coordinate axes. J_n is an exchange parameter about which there is some dispute. Many workers have used the third-order perturbation approach of Moriya,[34] and interpreted the J_n to be exchange integrals between ground and excited states. Gribnau and Keijzers,[35] however, have shown using a second-order perturbation theory that J_n is just the exchange integral between the triplet and singlet versions of the excited state. In the case of Cu(II)−Cu(II) and VO(IV)−VO(IV) dimers the J_n that is dominant is the one in which either the ground state or coupled excited state is the d_{xz} or d_{yz} that forms a σ bond with the bridging ligands. In the case of Cu(II)−Cu(II) and VO(IV)−VO(IV) dimers, in which the symmetry about the metal ion is six-coordinate, this involves an excited state and ground state that are both in the ML_2M plane and gives a D anisotropy and g anisotropy that is perpendicular to the plane. In our system this is not so. In the case of **1**, if it is assumed that the y axis is in the $TiCl_2Ti$ plane, then l_x couples the ground state with d_{yz}, producing the anisotropy in the exchange interaction to be along the x axis as was found above. Thus, this coordinate system is proposed for **1** (Figure 5).

(34) Moriya, T., Rado, G. T., Suhl, H., Eds. *Magnetism*; Academic Press: New York, 1963; Vol. 1, p 85.
(35) Gribnau, M. C. M.; Kreijzers, C. P. *Inorg. Chem.* **1987**, *26*, 3413−3414.

Extended Hückel MO Calculations. In an effort to examine the nature of the SOMOs for each of the Ti(III) centers in the dimer **1**, MO calculations of metallocene and monocyclopentadienyl ligand complexes are considered. In the now classic work of Hoffmann and Lauher,[36] the LUMO for Cp_2TiCl_2 is described as the $1a_1$ orbital, of d_{z^2} symmetry, in the $TiCl_2$ plane. On the basis of this description, the HOMO of the corresponding Ti(III) dimer $[Cp_2Ti(\mu\text{-}Cl)]_2$ (**5**) is predicted to be the admixture of two such metal-based orbitals, providing a MO in the Ti_2Cl_2 plane and along the Ti−Ti vector (Figure 5). Previously reported MO calculations (FHMO) for $CpTiCl_3$ revealed that the three lowest energy unoccupied molecular orbitals are of 1e and $1a_1$ symmetry and are of primarily metal d_{xy}, $d_{x^2-y^2}$, and d_{z^2} character.[37] Related EHMO calculations have been performed for the Ti(IV) model $CpTi(NPH_3)Cl_2$ (**3**). LUMO, LUMO + 1, and LUMO + 2 are similar in form to those described above; however, the presence of the phosphinimide ligand disrupts the symmetry, removing the degeneracy of 1e unoccupied molecular orbitals. The LUMO in **3** is primarily a Ti-based d orbital with a smaller contribution from the N p orbital. Employing the present internal coordinate system, this orbital is of $d_{z^2-x^2}$ symmetry (Figure 5a), while the LUMO + 1 (Figure 5b) and LUMO + 2 (Figure 5c) are of d_{xy} and d_{z^2} character, respectively. Drawing an inference from these results predicts that the HOMO for the Ti(III) dimer would be comprised primarily of the $d_{z^2-x^2}$ on each of the two Ti(III) centers (Figure 5d,e). This extension is consistent with the symmetry of the HOMO predicted by the single-crystal EPR data described above. As well, the minor N p antibonding contributions to the HOMO are consistent with the lengthening of the Ti−N distance observed in **1**.

(36) Lauher, J. W.; Hoffman, R. *J. Am. Chem. Soc.* **1976**, *98*, 1729.
(37) Nadasdi, T. T.; Huang, Y.; Stephan, D. W. *Inorg. Chem.* **1993**, *32*, 347−356.

Conclusion

The synthesis and structure of the dimeric Ti(III) **1** have been established. The results of the first single-crystal EPR study of a Ti(III) dimer, **1** has elucidated both the **g** matrix and zero-field parameters. Interpretation of these data is consistent with the results of EHMO calculations that infer a HOMO comprised of principally metal d orbitals that are approximately orthogonal to the Ti−Ti vector. These results illustrate that while phosphinimide ligands may be considered steric analogues to cyclopentadienyl ligands, electronically these ligands are distinct.

Acknowledgment. Financial support from the NSERC of Canada and NOVA Chemicals Corp. is gratefully acknowledged.

Supporting Information Available: X-ray crystallographic files in CIF format for the structure of **1**. This material is available free of charge via the Internet at http://pubs.acs.org.

IC991305L